ISSN: 1410-8917
e-ISSN: 2597-9914

Jurnal Kimia Sains dan Aplikasi 26 (9) (2023): 353-362

Jurnal Kimia Sains dan Aplikasi
Journal of Scientific and Applied Chemistry

Journal homepage: http://ejournal.undip.ac.id/index.php/ksa

Development of Microfluidic Paper-Based Analytical Devices (µPADs) for Determination of Cd^{2+}, Pb^{2+}, and Cu^{2+} Ions in Mineral Water

Andri Hermansyah [1,2], Neil V. Rees [3], Jarnuzi Gunlazuardi [1], Rahmat Wibowo [1,*]

[1] Department of Chemistry, Faculty of Mathematics and Natural Sciences, University of Indonesia, Depok, 16424, Indonesia
[2] Indonesian Food and Drug Authority, Jakarta 10560, Indonesia
[3] School of Chemical Engineering, University of Birmingham, Edgbaston, Birmingham B15 2TT, United Kingdom

* Corresponding author: rahmat.wibowo@sci.ui.ac.id

https://doi.org/10.14710/jksa.26.9.353-362

Article Info

Article history:

Received: 01st September 2023
Revised: 07th November 2023
Accepted: 10th November 2023
Online: 30th November 2023

Keywords:
dual detection systems; hot embossing; microfluidic paper-based analytical devices; RGB sensor; screen printing; square wave anodic stripping voltammetry

Abstract

Microfluidic paper-based analytical devices (µPADs) have been successfully developed using dual detection: electrochemical and colorimetric systems. The µPADs have the potential to be used as Pb(II), Cd(II), and Cu(II) sensors to test the quality of water. The fabrication process uses hot embossing and screen-printing methods. The working electrode in the electrochemical zone was enhanced by the bismuth metal deposition process, while in the colorimetric zone, the gold nanoparticles modified with thioctic acid and dansylhydrazine (TA-Au-DNS) were used as a colorimetric sensor to detect Cu. The basic material of µPADs was characterized using a Fourier-transform infrared (FTIR) and a contact angle meter (CAM). In the electrochemical zone, the signals of square wave anodic stripping voltammetry (SWASV) resulted in good detection of Pb(II) and Cd(II) (from 0 to 100 ppb) with a limit of detection of 1.588 and 1.42 ppb, respectively. In the colorimetric zone, the performance of TA-Au-DNS for detecting Cu metal was obtained from readings through the red-green-blue (RGB) sensor as a miniature of µPADs reader. The LOD, LOQ, and average Vx_0 (linearity values) in the detection of Cu(II) (from 58 to 100 ppb) are 8.51 ppb, 28.36 ppb, and 0.41%, respectively.

1. Introduction

Heavy metal ions have consistently posed a significant concern in environmental pollution, particularly in our daily drinking water supply. Although the detrimental impacts of heavy metal contamination on human health are not immediately perceptible, continuous consumption over time leads to the accumulation of these contaminants within our bodies, surpassing safe concentration levels and resulting in severe health issues. Notably, among the various heavy metal pollutants, cadmium (Cd), lead (Pb), and copper (Cu) stand out due to their potential to cause fatal harm to humans [1, 2, 3, 4]. Due to the significant health risks associated with the presence of heavy metal contaminants such as copper (Cu), cadmium (Cd), and lead (Pb) in mineral water, the World Health Organization (WHO) has established stringent safety thresholds for these metals in drinking water. WHO specifically recommends a maximum allowable concentration of 0.01 mg/L for Pb, 0.003 mg/L for Cd, and 2 mg/L for Cu [5]. Various analytical techniques like Atomic Absorption Spectrometry (AAS), Inductively-Coupled Mass Spectroscopy (ICP-MS), Inductively-Coupled Atomic Emission Spectroscopy (ICP-AES), and Inductively-Coupled Plasma Optical Emission Spectroscopy (ICP-OES) have proven effective with favorable detection limits [6], there is a growing need for a more straightforward, more efficient method for early detection in the field. In this context, electrochemical sensors emerge as a highly promising alternative. Notably, these sensors offer several advantages, including their avoidance of complex sample preparation, minimal requirement for sophisticated electronic equipment, ease of setup and operation, real-time data provision, and flexibility in sampling locations [7].

A widely explored electrochemical sensor variant is the paper-based analytical devices (PADs), which are characterized by a paper-based substrate. PAD sensors exhibit versatility in applications, including tumor cell detection [8] and quantification of heavy metals and glucose content [9]. They can assume various shapes and benefit from diverse electrode preparation methods like stencil printing, inkjet printing, screen printing, and wax printing [10, 11]. In parallel with advancements in applications and fabrication techniques, ongoing research is dedicated to enhancing the functional properties of the paper substrate within PADs. This paper serves as the primary medium for binding metal ions and is subject to ongoing refinement and optimization [11]. One approach to augment heavy metal adsorption entails modifying the electrodes within PAD electrochemical sensors through a process known as bismuth metal electrodeposition [12]. This effort seeks to improve the sensor's performance in capturing heavy metal ions effectively.

Paper microfluidic devices combining several functions require different pathways to transport each liquid. Various fabrication techniques have been developed for this purpose: screen printing techniques, wax immersion or impregnation, 2D forming or cutting (e.g., blade plotter, CO_2 laser cutting), and 3D packaging or stacking (with origami paper). Several laboratory-scale methods such as photolithography, polydimethylsiloxane (PDMS) printing, inkjet etching, printed circuit, and plasma/laser treatment have also been developed to make paper microfluidics; however, these methods use quite complicated procedures, and the equipment is relatively expensive [9, 13, 14, 15]. Several fabrication techniques for paper microfluidics can be seen in Table 1.

Chaiyo *et al.* [16] introduced a noteworthy advancement in analytical technology: paper-based microfluidic analysis devices (µPADs) equipped with dual detection capabilities, namely electrochemical and colorimetric systems. The electrochemical component facilitates the quantification of lead (Pb) and cadmium (Cd) utilizing a modified diamond electrode incorporating bismuth and boron (Bi-BDDE). Simultaneously, colorimetric detection aids in determining copper (Cu) concentrations by capitalizing on the catalytic etching of silver nanoparticles (AgNPs) through thiosulfate ($S_2O_3^{2-}$). Unfortunately, the fabrication process of this sensor entails complexity and employs relatively expensive materials. Hence, there is a growing demand for alternative approaches that maintain its functionality while reducing production costs.

Postulka *et al.* [17] achieved a significant breakthrough by creating hydrophilic and hydrophobic pathways in paper microfluidics through the hot embossing method. This method represents a faster and more efficient approach to creating fluid pathways on µPADs. Furthermore, Nath *et al.* [2] successfully developed a gold nanosensor modified with thioctic acid and dansylhydrazine (TA-Au-DNS), then printed on paper. This sensor demonstrated the ability to rapidly detect Cu^{2+} ions, even at very low concentrations in solution. The TA-Au-DNS sensor introduces a novel technique with potential applications in developing colorimetric sensors on µPADs.

The hot embossing technique was employed to develop µPADs featuring dual detection capabilities: electrochemical and colorimetric. This study used carbon and silver ink with a fabrication process using reasonably simple equipment. Carbon electrodes have several advantages, such as low background current, inertness, low production costs, and a large potential window [18]. This study used AuNPs material for colorimetric sensors because it is non-toxic and easier to modify by combining functional ligands such as thioctic acid, which can detect transition metal ions such as Cu^{2+} [2, 19].

Table 1. Several types of µPADs with their fabrication techniques, analytical methods, and analytes measured

Working Electrode	Fabrication	Detection Method	Samples	Detection limit	Reference
Carbon, Bi	photolithography, screen-printing	ASV	Pb^{2+}	1 ppb	[9]
Graphite	Wax-printing, screen-printing	SWV	Cd^{2+} Pb^{2+}	11 ppb 7 ppb	[13]
Graphite foil	Cutting, stacking	SWV	Cd^{2+} Pb^{2+}	1.2 ppb 1.8 ppb	[14]
Ru@AuNPs and Si@CNCs conjugated DNA strands	Wax-printing, screen-printing	ECL	Pb^{2+} Hg^{2+}	10 pM 0.2 nM	[15]
Bi-BDDE and AgNPs-$S_2O_3^{2-}$	Wax-printing, screen-printing	ASV	Cd^{2+} Pb^{2+} Cu^{2+}	0.1 ppb 0.1 ppb 4.12 ppt	[16]
Carbon, Bi, and TA-AU-DNS	Hot embossing, screen-printing	SWASV	Cd^{2+} Pb^{2+} Cu^{2+}	1.588 ppb 1.42 ppb 8.51 ppb	Present work

Ru@AuNPs: Ru(bpy)3 2þ-gold nanoparticle, Si@CNCs: carbon nanocrystals capped silica nanoparticles, ASV: Anodic stripping voltammetry, ECL: electrochemiluminescence, ND: Not defined.

Research carried out by Nath *et al.* [2] showed that the TA-AU-DNS sensor is capable of detecting Cu^{2+} ions up to 1 ppb and produces quite clear color changes that are possible to measure using an RGB sensor by utilizing microcontroller technology, which is proposed as a miniature sensor reader. These µPADs serve as analytical tools for assessing the presence of lead (Pb), cadmium (Cd), and copper (Cu) metal contamination in water samples. Within the electrochemical detection region, bismuth electrodeposition was utilized for Pb and Cd metal detection, whereas in the colorimetric detection zone, TA-Au-DNS was used to detect Cu metal.

2. Experimental

2.1. Materials and Instrument

The ingredients used in this research include: Paraffin pastillen (1.07164.2500), Potassium chloride (1.04936.1000), Potassium ferricyanide (1.04973.0250), Acetic acid (glacial) 100%, Sodium acetate (1.06268.1000), Dimethyl sulfoxide (1.02952.1000), standard solution 1000 ppm ($Pb(NO_3)_2$, $Cd(NO_3)_2$, $Cu(NO_3)_2$, $Bi(NO_3)_3$, $Fe(NO_3)_3$, $Cr(NO_3)_3$, $Zn(NO_3)_2$ and Arsenic acid), Sodium tetrachloroaurate (III) dihydrate ($NaAuCl_4.2H_2O$) 99%, Thioctic acid, Dansylhydrazine (DNS) 98%, Sodium citrate dihydrate ≥ 99.0%, Ethylcarbodiimide hydrochloride (EDC) ≥ 99.0% from Merck and SIGMA-ALDRICH, NHS (N-hydroxysuccinimide) 97-103% from HiMedia Laboratories, Whatman No.1 paper with a diameter of 150 mm from GE Healthcare as well as carbon ink (Max Shield) and silver ink (MJ Chemical) with a resistance value of 0-5 Ohm/cm² purchased online. All solutions were prepared using deionized water with a resistivity of 18.2 MOhm.cm from Milli-Q Merck. In this study, several instrumentations were also used, including a potentiostat (e-DAQ Model ED401), FTIR (Shimadzu IR Prestige-21), UV-Spectrophotometer Vis (Thermo Scientific, Multiskan Go), and Contact Angle Meter (OCA 25, NORLEQ).

2.2. Procedures

2.2.1. Manufacturing of µPADs

The proposed µPADs consisted of several main components, including the electrochemical detection zone, colorimetric detection zone, sample flow path, and absorbance pad. The hydrophobic pattern was printed on Whatman 1 filter paper using paraffin with a hot embossing mechanism or tracing an embossed layer on the surface by heating at a temperature of 65–75°C [17]. The paper and paraffin layers were arranged on a patterned steel plate during the heating process, as depicted in Figure 1a. Subsequently, a flat glass was applied to the top of the paper with a load of approximately 1-2 kg. This pressure helped guide the molten paraffin onto the paper, facilitating the formation of the desired hydrophilic and hydrophobic layers. Whatman 1 chromatography paper was selected due to its better porosity, flow rate, and sample retention capabilities than other paper types [20]. Whatman Paper 1 has gained widespread recognition for its efficacy in developing paper-based microfluidic sensors, as demonstrated in prior research studies [10, 12, 21, 22].

The three electrodes were fashioned upon patterned paper in the electrochemical detection zone through the screen-printing method. Carbon ink served the dual role of the working and supporting electrodes, whereas silver ink fulfilled the role of the reference electrode. The electrode body was enveloped by copper foil to prevent electrode displacement [16]. Figure 1 illustrates the employment of hot embossing and screen printing methods in this process.

Within the realm of colorimetric detection, a µPADs colorimetric sensor was prepared by stepwise chemical conjugation of gold nanoparticles (AuNPs) with thioctic acid (TA) followed by fluorescent dansylhydrazine (DNS) molecules in the presence of the coupling agent, 1-ethyl-3-[3- (dimethylamino)propyl]carbo-diimide (EDC) and N-hydroxysuccinimide (NHS). Initially, 10 mL of stabilized gold nanoparticle citrate was prepared by blending 50 µL of 0.1 M $NaAuCl_4.2H_2O$ with 5 mg of sodium citrate dissolved in 1 mL of deionized (DI) water. This mixture was then heated to 90°C while stirring, leading to a noticeable transformation of the solution color into a vibrant red hue, signifying the formation of gold nanoparticles (AuNPs). Subsequently, 3 mg of thioctic acid dissolved in 1 mL of methanol was introduced into the 10 mL of citrate AuNPs, with subsequent pH adjustment to 8.0. The resulting mixture was stirred at room temperature for 8 hours. Unbound thioctic acid was subsequently eliminated via centrifugation at 9000 rpm for 10 minutes.

The process continued with the dissolution of thioctic acid (TA)-conjugated gold nanoparticle pellets in 5 mL of water to start the second conjugation step involving dansylhydrazine. In this phase, 10 mM EDC and 10 mM NHS liquids were taken 200 µL each and were incorporated into the 5.0 mL TA-Au solution. The ensuing solution was gently stirred for one hour at room temperature, yielding a TA-Au-EDC/NHS solution. Subsequently, 7 mg of dansylhydrazine was introduced into a mixture of 1 mL dimethyl sulfoxide (DMSO) and deionized water, then added to the 5 mL TA-Au-EDC/NHS mixture. This blend was stirred for 3 hours at room temperature, during which any excess DNS was later eliminated via centrifugation at 9000 rpm for 10 minutes. The resulting modified gold nanoparticles were then applied to the colorimetric zone of the µPADs, as illustrated in Figure 2.

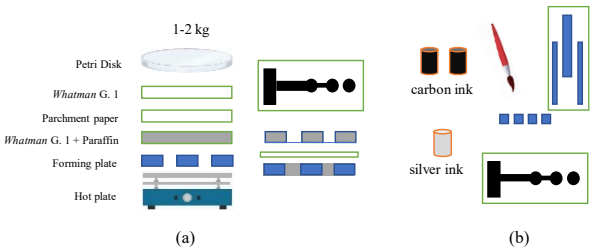

Figure 1. µPADs fabrication technique, (a) hot embossing technique, (b) screen printing technique

2.2.2. Characterization of µPADs

The performance of µPADs depends on several key parameters, including the electrode material, paper type, electrode fabrication technique, fluid flow control, sensor design, and signal amplification method [11]. In this research, the characterizations of µPADs were conducted, including assessing the base material (hydrophobic and hydrophilic layers) of the resulting µPADs using FTIR and CAM, examining the active electrode surface in the electrochemical detection zone, and characterizing TA- Au-DNS using FTIR.

3. Results and Discussion

3.1. Morphology of µPADs

Figure 2 presents the outcomes of µPAD fabrication. It is evident from the figure that the µPADs exhibit well-formed hydrophobic and hydrophilic pathways. Notably, the hydrophilic layer is 4 mm wide, leading toward the electrochemical detection zone, while a 2 mm width directs it to the colorimetric detection zone. This design strategically controls the sample flow rate, ensuring faster movement toward the electrochemical detection zone. This separation is crucial to prevent the sample from mixing with gold nanoparticles in the colorimetric detection zone during electrochemical analysis. The objective is to guarantee that the sample reaches the colorimetric zone only after completing the electrochemical detection process. Additionally, the second colorimetric detection zone is a reference for comparing the TA-Au-DNS color before Cu^{2+} ion detection. Lastly, the absorbent pad serves the dual purpose of directing sample flow and collecting waste materials after electrochemical analysis. These design elements collectively optimize the functionality of the µPADs.

Figure 3 displays the FTIR results concerning the hydrophobic and hydrophilic layers of the resulting µPADs. Spectrum (a) represents the spectrum of Whatman 1 paper coated with paraffin, while spectrum (b) showcases the pure Whatman 1 paper lacking paraffin coating. Spectrum (c) corresponds to the paraffin spectrum itself. Figure 3c shows that the paraffin spectra unmistakably confirm the existence of C–H stretching vibrations at wavenumbers 2916 cm^{-1} and 2842 cm^{-1}. Additionally, infrared absorption is evident in C–H bond vibrations at wavenumbers 1461 cm^{-1} and 1375 cm^{-1}. Furthermore, the vibration of the CH_2 absorption band is notably affirmed at a wavenumber of 718 cm^{-1}, indicating the presence of an aliphatic structure inherent to paraffin [23].

The FTIR spectra of the Whatman 1 paper (before and after being coated with paraffin) exhibit striking similarities. In both cases, characteristic features are observed, such as O-H stretching vibrations at the wavenumber range of 3135–3560 cm^{-1} and C-H stretching group vibrations within the range of 2824–2983 cm^{-1}. Furthermore, IR absorption is evident at a wavenumber of 1640 cm^{-1}, corresponding to the stretching of the -CO bond found in the aldehyde group of cellulose. Additionally, absorptions between wavenumbers 1000–1200 cm^{-1} signify the presence of an ether group. Notably, wavenumbers ranging from 500–700 cm^{-1} represent the distinctive fingerprint of C-H vibrations [24, 25]. This collective data demonstrates the suitability of the paraffin used for creating the hydrophobic layer in µPAD fabrication. Importantly, it does not interfere with the active groups of cellulose compounds, which constitute the primary components of the paper. This compatibility makes paraffin an excellent choice for this purpose.

The hydrophobic coating on µPADs was validated using a Contact Angle Meter (CAM). This examination assessed the hydrophobic layer's ability to repel liquids to identify the optimal rate and direction of flow for the sample to be tested. Figure 4 displays the outcomes of CAM tests conducted on the hydrophobic layer of µPADs. As illustrated in Figure 4, the contact angles of the µPADs' hydrophobic layer were measured at three distinct points: 102.9° at location 1, 106.4° at location 2, and 103.7° at location 3. These findings unequivocally confirm the hydrophobic properties of the tested layer, as all measured contact angles fall within the range of 90° to 120° [26].

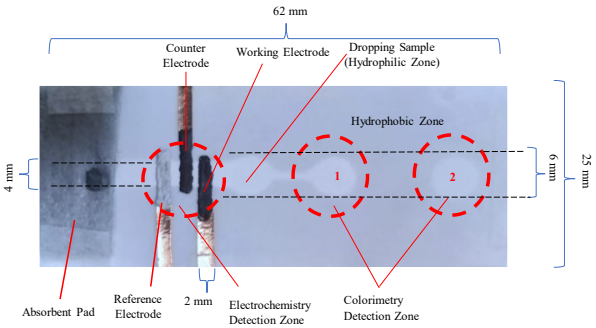

Figure 2. Cross-section of the resulting µPADs

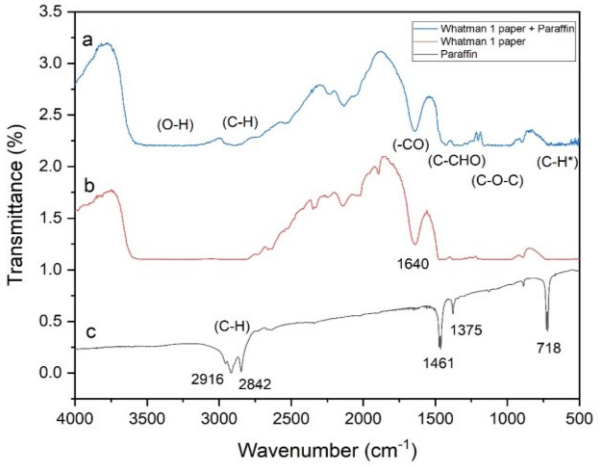

Figure 3. FTIR spectra of the hydrophobic and hydrophilic layers of the resulting µPADs

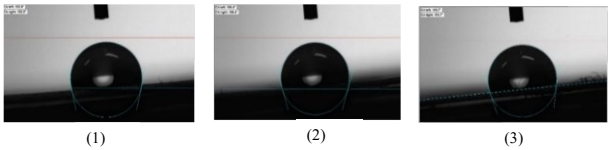

Figure 4. Results of measuring the contact angle of the hydrophobic layer at three different location points using a Contact Angle Meter (CAM)

3.2. Electrochemical Surface Area

The objective of calculating the surface area of the working electrode in µPADs is to assess its electrochemical reactivity. Typically, an electrode's electroactive surface area surpasses its geometric surface area. This discrepancy arises from microscopic features like pores, roughness, and irregularities on the electrode surface, leading to an expanded effective surface area. However, there are instances where the electroactive surface area might be less than the geometric surface area. This occurs when certain portions of the electrode's surface are non-conductive, rendering them ineffective for facilitating electrochemical reactions [27].

The experiment measured electrode surface area utilizing a 5 mM $K_3Fe(CN)_6$ solution in a 0.1 M KCl solution through cyclic voltammetry. Experiments were conducted in the potential range of -1000 to +1000 mV with varying scan rates of 5, 10, 25, 50, and 100 mV/s, resulting in a cyclic voltammogram of µPADs (Figure 5a). The choice of the $K_3Fe(CN)_6$ solution was based on its straightforward preparation process and stability and its reversible (nearly to 1) anodic and cathodic currents in testing all types of electrodes. The chosen potential range was motivated by the estimated standard reduction potential of a 5 mM $K_3Fe(CN)_6$ solution at 361 ± 0.5 mV. Furthermore, an upper limit of -1150 mV was set to prevent the oxidation of dissolved oxygen, which could disrupt the diffusion process [28, 29].

The electrode's electroactive surface area is ascertained using the Randles-Sevcik equation, a mathematical expression linking the peak oxidation current (on the y-axis) with the square root of the scan rate (on the x-axis) [30, 31]. Figure 5 shows the cyclic voltammogram of µPADs (a) and the curve plot of I against $(\nu)^{1/2}$ (b) at varying scan rates of 5-100 mV/s. As depicted in Figure 5, the cyclic voltammogram exhibits a notably linear profile, effectively portraying the oxidation-reduction process transpiring on the electrode surface through a diffusion process. This is of significant importance as it signifies the electrochemical activity of the electrode. The correlation between scan rate and current response is apparent: as the scan rate increases, the current response concurrently escalates. This relationship is attributed to the accelerated electron transfer rate facilitated by higher scan rates. Consequently, ions diffuse more proficiently across the µPADs' electrode surface, culminating in the formation of thicker diffusion layers. This augmented diffusion layer thickness contributes to the amplification of the resulting current response.

Conversely, lower scan rates yield diminished current responses due to the formation of fewer diffusion layers [30]. Furthermore, Figure 5a elucidates that the discrepancy between the anodic peak potential and the cathodic peak potential, often called peak-peak separation, exceeds 60 mV, signifying quasi-reversible conditions. The Randles-Sevcik equation was employed to ascertain the active surface area of the working electrode under such circumstances (Equation (1)).

$$I_p^a = \pm 0.436\ \mathrm{nFAC}\sqrt{\frac{nFD\nu}{RT}} \quad (1)$$

where, I is the peak oxidation current, n is the number of electrons involved during the reaction, A is the electrode surface area, D is the diffusion coefficient, C is the bulk concentration, ν is the scan rate used, F is Faraday's constant (96485 $Cmol^{-1}$), R is the ideal gas constant (8.314 $Jmol^{-1}K^{-1}$), and T is the observation temperature (K) [32].

According to the plot of current (I) vs. $(\nu)^{1/2}$ plot (Figure 5b), the calculated surface area of the µPADs working electrode is 0.031 cm^2. In contrast, geometric calculations yield a larger surface area of 0.08 cm^2. These findings reveal that the active surface area of the µPADs working electrode is smaller than its geometric counterpart. This discrepancy arises due to non-conductive regions on the working electrode's surface, rendering them ineffective in promoting electrochemical reactions. Consequently, these non-conductive areas reduce the electrochemically active surface area [27]. The electron charge transfer behavior of the µPADs can be performed with impedance analysis [33]. This can be used as a suggestion for further research and, unfortunately, is not discussed in our paper.

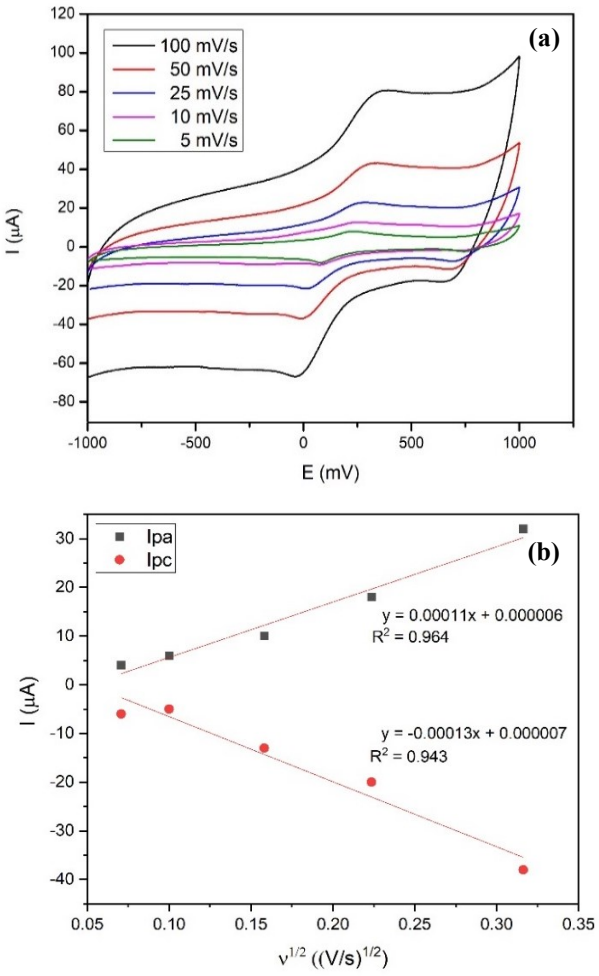

Figure 5. (a) Cyclic voltammogram of µPADs using 5 mM $K_3Fe(CN)_6$ containing 0.1 M KCl at various scan rates, and (b) curve plot of I against $(\nu)^{1/2}$

3.3. Colorimetric Sensor Characterization

Figure 6 presents the infrared spectra of different samples: (a) gold nanoparticles before conjugation ($NaAuCl_4$), (b) gold nanoparticles with thioctic acid (TA- Au), and (c) gold nanoparticles with thioctic acid and DNS (TA-Au-DNS). In Figure 6, all gold nanoparticles exhibit infrared absorption within the wavenumber range of 3200 3700 cm^{-1}, characterized by varying intensities and widths. This absorption corresponds to the stretching vibration of O-H groups on the gold nanoparticles. However, in the case of TA-Au-DNS, an enhancement in intensity is evident at a specific wavelength, 1636 cm^{-1}, indicating the presence of the C=O stretching group in the amide.

Additionally, spectral features represent symmetric and asymmetric COO^- stretching in sodium citrate at wavelengths 1399 cm^{-1} and 1585 cm^{-1}, respectively. Intriguingly, in the IR spectrum of TA-Au-DNS, these peaks have shifted to 1311 cm^{-1} and 1432 cm^{-1}, suggesting the formation of citrate groups on the surface of the nanoparticles, signifying the creation of new compounds [34]. Furthermore, conspicuous increases in IR absorption intensity at wavelengths 945 cm^{-1} and 1017 cm^{-1} are observed when transitioning from TA-Au to TA-Au-DNS, implying the formation of novel functional groups, which may serve as attachment points for other substances, particularly heavy metal samples in future detection applications.

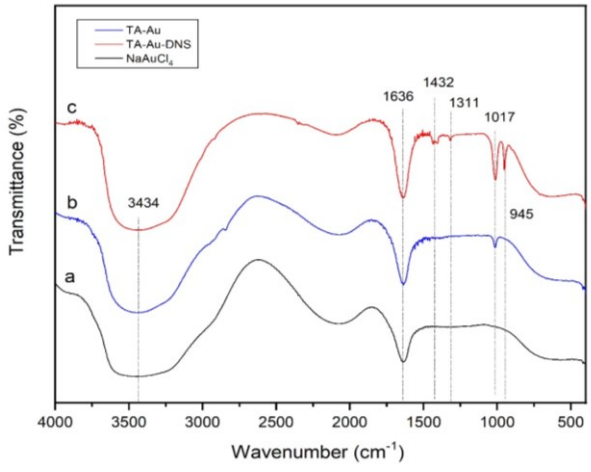

Figure 6. FTIR spectra of (a) $NaAuCl_4$, (b) TA-Au, and (c) TA-Au-DNS

3.4. Performance of µPADs

The performance evaluation of the electrochemical detection zone in µPADs is demonstrated through testing for cadmium (Cd) and lead (Pb) metals in mineral water samples with concentrations ranging from 0 to 100 ppb. The experiment involved dispensing 50 µL of the sample solution using the Square Wave Anodic Stripping Voltammetry (SWASV) method, with a potential range of -1400 to 800 mV, employing a scan rate of 125 mV/s and a frequency of 25 Hz. The deposition of 500 ppb bismuth metal was conducted at -1400 mV for 60 seconds. The measurements were repeated thrice, averaged, and used to generate a stripping voltammogram and a calibration curve for Pb and Cd, as illustrated in Figure 7.

The results depicted in Figure 7 reveal a notable trend: as the concentration of Cd and Pb increases, the peak stripping current also rises. The calibration curves for Cd and Pb exhibit a reasonably linear relationship, with correlation coefficients of 0.9522 for Cd and 0.9716 for Pb. Sample measurements employed the standard additions method, initially incorporating 5 ppb of Pb and Cd metals as sample blanks for subsequent detection by µPADs. Metal concentrations of 5, 15, 35, 55, 75, and 95 ppb were incrementally added to each sample blank to assess linearity.

Table 2 shows the relative standard deviation, accuracy, limit of detection (LOD), and limit of quantification (LOQ) from measurements of Pb and Cd metals in mineral water with a concentration range (0– 100). These values are obtained from Equations (2-5).

$$\%\ RSD = \frac{SD}{\bar{X}} x\ 100\ \% \quad (2)$$

$$Recovery\ (Accuracy) = \frac{Cf-Cb}{Ca} x\ 100 \quad (3)$$

$$LOD = 3\ x\ SD \quad (4)$$

$$LOQ = 10\ x\ SD \quad (5)$$

where, SD is the standard deviation, $\bar{x}$ is the average data, Cf is the concentration obtained, Cb is the initial concentration of the sample, and Ca is the sample/standard added [35].

The determination of LOD (Limit of Detection) and LOQ (Limit of Quantification) values followed a standard addition approach, whereby a blank solution was augmented with 5 ppb of the metal mixture. Subsequently, three distinct concentrations representing the measurement range were prepared [36]. The LOD and LOQ values for Cd and Pb metals were computed by analyzing the average test results and employing a calibration curve. For Cd, the calculated values were 1.588 ppb (LOD) and 5.29 ppb (LOQ), while for Pb, they were 1.42 ppb (LOD) and 4.74 ppb (LOQ). From Table 2, it can also be seen that the results show a fairly good correlation between concentration and stripping current response.

Table 2. Results of determining Cd and Pb levels using µPADs sensors using the SWASV technique with Bi-metal deposition at a potential of -1400 mV for 60 seconds using 0.1 M ABS solution pH 4.5

	Cd	Pb
% RSD	29.21	38.89
% Recovery (Accuracy)	82.85	73.67
Correlation Factor (R^2)	0.9522	0.9716
LOD (ppb)	1.588	1.42
LOQ (ppb)	5.29	4.74

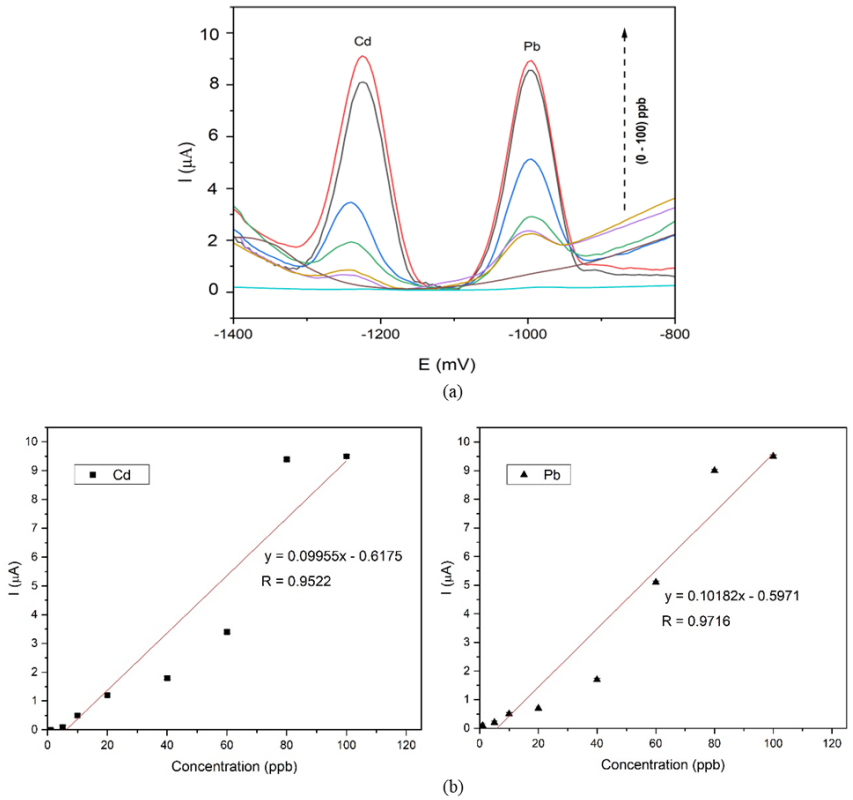

Figure 7. Stripping voltammogram of (a) mixture of 0–100 ppb Pb and Cd metals and (b) calibration curve of Cd and Pb in ABS 0.1 M pH 4.5 with 500 ppb Bi-metal deposition at a deposition potential of -1400 mV for 60 seconds using a μPADs sensor

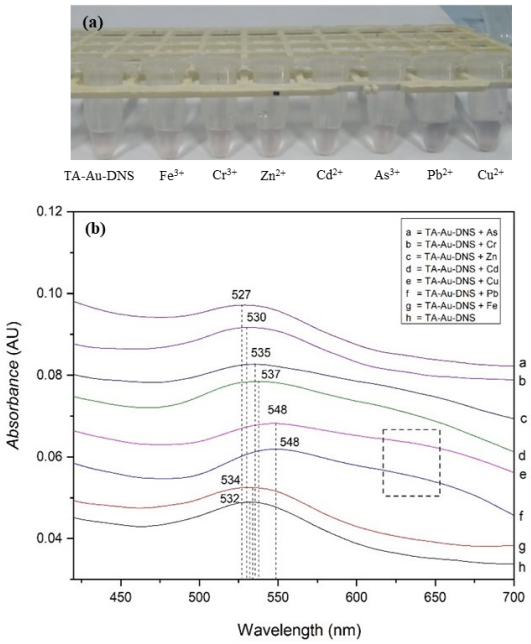

Figure 8. (a) Color response and (b) spectrum of TA-Au-DNS after being mixed with 10 ppm of metals (Fe^{3+}, Cr^{3+}, Zn^{2+}, Cd^{2+}, As^{3+}, Pb^{2+}, and Cu^{2+})

The performance of the colorimetric detection zone of μPADs was determined by examining the selectivity of the TA-Au-DNS gold nanosensor towards various metal ions, including Fe^{3+}, Cr^{3+}, Zn^{2+}, Cd^{2+}, As^{3+}, Pb^{2+}, and Cu^{2+}. Specifically, 0.1 mL of the TA-Au-DNS gold nanosensor was combined with 0.1 mL of each metal solution, each having a concentration of 10 ppm. The resultant color change resulting from the mixture of these solutions was visually observed, facilitating the determination of the nanosensor's selectivity towards the specified metal ions.

Figure 8 illustrates the spectrum of TA-Au-DNS after combining 0.1 mL of various metal samples, each with a concentration of 10 ppm. In Figure 8a, a specific response of TA-Au-DNS to samples containing 10 ppm of Pb^{2+} and Cu^{2+} ions is discernible, resulting in a color transition of TA-Au-DNS from pink to blue (purple). Figure 8b demonstrates that upon introducing Zn, Cd, As, Fe, and Cr metals, the visible spectrum of TA-Au-DNS persists within the wavelength range of 527–537 nm. Conversely, upon adding Pb and Cu metals, the spectrum of TA-Au-DNS undergoes a shift to a wavelength of 548 nm, accompanied by the emergence of absorption at wavelengths between 600–650 nm. This phenomenon shows the commencement of the aggregation process, coinciding with the shift to 548 nm.

Surface plasmon resonance (SPR) is a distinctive property exhibited by gold nanoparticles (AuNPs). This characteristic is influenced by several factors, including the size and shape of AuNPs particles and the dielectric properties of their environment. Changes in the distance between AuNPs particles induce variations in their dielectric characteristics. When Cu^{2+} ions are added, AuNPs ligands form bonds with these ions. Consequently, the initially dispersed AuNPs approach each other, leading to an increase in their size. This process gives rise to a phenomenon known as "interparticle surface plasmon coupling," resulting in a bathochromic shift of the SPR band of AuNPs from 520 nm to 650 nm (resulting in a color change from pink to blue) [37].

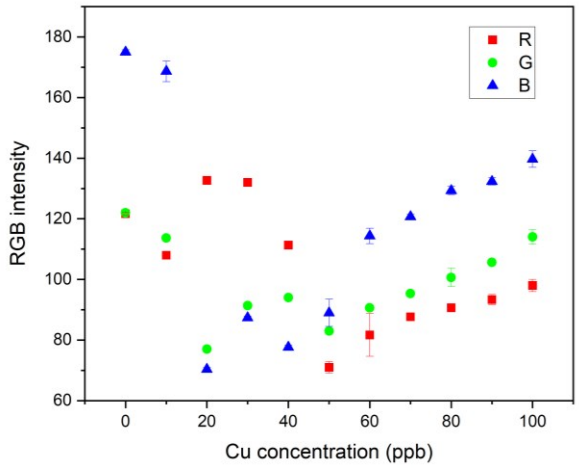

Figure 9. Response of the RGB sensor to the color change of TA-Au-DNS after adding Cu with a concentration of (0–100) ppb

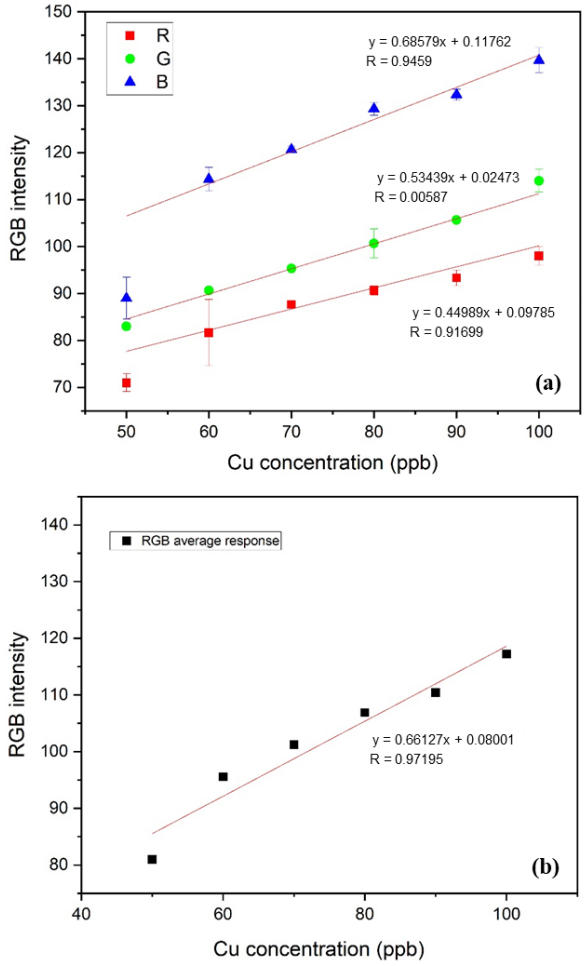

Figure 10. (a) RGB sensor response calibration curve and (b) average RGB response to changes in TA-Au-DNS after adding Cu with a concentration of (50–100) ppb

The performance of the colorimetric detection zone of the µPADs device was proceeded by monitoring color variations resulting from the addition of Cu^{2+} metal ions at varying concentrations (ranging from 0 to 100 ppb) to the TA-Au-DNS gold nanoparticle sensor. Subsequently, the resultant mixture is dispensed onto the colorimetric detection zone of the µPADs. After that, it is subjected to analysis by directing a polychromatic beam through the RGB sensor (TCS34725) incorporated within a microcontroller-based simulator.

Figure 9 illustrates the response of RGB sensor readings to changes in TA-Au-DNS following the addition of Cu at concentrations ranging from 0 to 100 ppb. As depicted in Figure 10, the obtained readings demonstrate a notable linearity within the Cu concentration range of 50 to 100 ppb. This linear relationship facilitates the generation of a calibration curve with a correlation coefficient (r) value of 0.97195, as shown in Figure 10b. The response emanating from the RGB sensor, integrated into a microcontroller-based simulator, currently exists as arbitrary units. Further development and in-depth discussion of this system conversion will be the focus of our forthcoming publication.

4. Conclusion

The dual detection µPADs sensor was effectively fabricated using the wax method, employing hot embossing and screen-printing techniques to produce a consistent hydrophobic and hydrophilic layer. Notably, the active surface of the µPADs working electrode is smaller than its geometric counterpart, as not all segments of the working electrode exhibit electroactivity, rendering them incapable of facilitating electrochemical reactions. Optimal conditions for Pb and Cd analysis in AMDK using 500 ppb Bi-modified µPADs entail electrodeposition at a potential of -1.4 V for 60 seconds, employing a 0.1 M ABS solution at pH 4.5, without the presence of Cu metal. Within the concentration range of 0–100 ppb, the LOD and LOQ values for Cd metal were determined as 1.58 ppb and 5.29 ppb, respectively, while for Pb metal, they were found to be 1.42 ppb and 4.74 ppb. Furthermore, the successful synthesis and application of the TA-Au-DNS sensor in the colorimetric detection zone of µPADs demonstrates its sensitivity in detecting Cu^{2+} ions within the 50–100 ppb concentration range. The LOD, LOQ, and average Vx_0 (linearity values) are 8.51 ppb, 28.36 ppb, and 0.41%, respectively. See the supporting documents for more details on determining LOD, LOQ, and Vx0. Additionally, creating the µPADs sensor simulator (reader) holds the potential for further development into a dual-detection (electrochemical and colorimetric) potentiostat simulator. According to the threshold values for Pb, Cd, and Cu metal contamination in drinking water established by the WHO, the resultant µPADs sensor meets the requisite detection limits, rendering it suitable for detecting Cd and Pb metals within the 0–100 ppb concentration range, while Cu in the range 58–100 ppb.

References

[1] Jillian E. Gall, Robert S. Boyd, Nishanta Rajakaruna, Transfer of heavy metals through terrestrial food webs: a review, *Environmental Monitoring and Assessment*, 187, (2015), 201 https://doi.org/10.1007/s10661-015-4436-3

[2] Peuli Nath, Ravi Kumar Arun, Nripen Chanda, Smart gold nanosensor for easy sensing of lead and copper ions in solution and using paper strips, *RSC*

Advances, 5, 84, (2015), 69024-69031 https://doi.org/10.1039/C5RA14886C

[3] Mehrdad Rafati-Rahimzadeh, Mehravar Rafati-Rahimzadeh, Sohrab Kazemi, Aliakbar Moghadamnia, Cadmium toxicity and treatment: An update, *Caspian Journal of Internal Medicine*, 8, 3, (2017), 135-145 http://dx.doi.org/10.22088/cjim.8.3.135

[4] Karl E. Mason, A Conspectus of Research on Copper Metabolism and Requirements of Man, *The Journal of Nutrition*, 109, 11, (1979), 1979-2066 https://doi.org/10.1093/jn/109.11.1979

[5] World Health Organization, Guidelines for drinking-water quality, 3rd edition: Volume 1 - Recommendations incorporating the first and second addenda, 1, (2008),

[6] Rajneet Kour Soodan, Yogesh B. Pakade, Avinash Nagpal, Jatinder Kaur Katnoria, Analytical techniques for estimation of heavy metals in soil ecosystem: A tabulated review, *Talanta*, 125, (2014), 405-410 https://doi.org/10.1016/j.talanta.2014.02.033

[7] Ulrich Guth, Winfried Vonau, Jens Zosel, Recent developments in electrochemical sensor application and technology—a review, *Measurement Science and Technology*, 20, 4, (2009), 042002 https://doi.org/10.1088/0957-0233/20/4/042002

[8] Panpan Wang, Lei Ge, Mei Yan, Xianrang Song, Shenguang Ge, Jinghua Yu, Paper-based three-dimensional electrochemical immunodevice based on multi-walled carbon nanotubes functionalized paper for sensitive point-of-care testing, *Biosensors and Bioelectronics*, 32, 1, (2012), 238-243 https://doi.org/10.1016/j.bios.2011.12.021

[9] Zhihong Nie, Christian A. Nijhuis, Jinlong Gong, Xin Chen, Alexander Kumachev, Andres W. Martinez, Max Narovlyansky, George M. Whitesides, Electrochemical sensing in paper-based microfluidic devices, *Lab on a Chip*, 10, 4, (2010), 477-483 https://doi.org/10.1039/B917150A

[10] Liu-Liu Shen, Gui-Rong Zhang, Bastian J. M. Etzold, Paper-Based Microfluidics for Electrochemical Applications, *ChemElectroChem*, 7, 1, (2020), 10-30 https://doi.org/10.1002/celc.201901495

[11] Mahroo Baharfar, Mohammad Rahbar, Mohammad Tajik, Guozhen Liu, Engineering strategies for enhancing the performance of electrochemical paper-based analytical devices, *Biosensors and Bioelectronics*, 167, (2020), 112506 https://doi.org/10.1016/j.bios.2020.112506

[12] Jianjun Shi, Fan Tang, Honglong Xing, Huxiang Zheng, Bi Lianhua, Wang Wei, Electrochemical detection of Pb and Cd in paper-based microfluidic devices, *Journal of the Brazilian Chemical Society*, 23, 6, (2012), 1124-1130 https://doi.org/10.1590/S0103-50532012000600018

[13] Mariana Medina-Sánchez, Miquel Cadevall, Josep Ros, Arben Merkoçi, Eco-friendly electrochemical lab-on-paper for heavy metal detection, *Analytical and Bioanalytical Chemistry*, 407, (2015), 8445-8449 https://doi.org/10.1007/s00216-015-9022-6

[14] Liu-Liu Shen, Gui-Rong Zhang, Wei Li, Markus Biesalski, Bastian J. M. Etzold, Modifier-Free Microfluidic Electrochemical Sensor for Heavy-Metal Detection, *ACS Omega*, 2, 8, (2017), 4593-4603 https://doi.org/10.1021/acsomega.7b00611

[15] Meng Zhang, Lei Ge, Shenguang Ge, Mei Yan, Jinghua Yu, Jiadong Huang, Su Liu, Three-dimensional paper-based electrochemiluminescence device for simultaneous detection of Pb^{2+} and Hg^{2+} based on potential-control technique, *Biosensors and Bioelectronics*, 41, (2013), 544-550 https://doi.org/10.1016/j.bios.2012.09.022

[16] Sudkate Chaiyo, Amara Apiluk, Weena Siangproh, Orawon Chailapakul, High sensitivity and specificity simultaneous determination of lead, cadmium and copper using μPAD with dual electrochemical and colorimetric detection, *Sensors and Actuators B: Chemical*, 233, (2016), 540-549 https://doi.org/10.1016/j.snb.2016.04.109

[17] Niels Postulka, Andreas Striegel, Marcel Kraußе, Dario Mager, Dieter Spiehl, Tobias Meckel, Matthias Worgull, Markus Biesalski, Combining Wax Printing with Hot Embossing for the Design of Geometrically Well-Defined Microfluidic Papers, *ACS Applied Materials & Interfaces*, 11, 4, (2019), 4578-4587 https://doi.org/10.1021/acsami.8b18133

[18] Wulan Tri Wahyuni, Budi Riza Putra, Achmad Fauzi, Desi Ramadhanti, Eti Rohaeti, Rudi Heryanto, A Brief Review on Fabrication of Screen-Printed Carbon Electrode: Materials and Techniques, *Indonesian Journal of Chemical Research*, 8, 3, (2021), 210-218 https://doi.org/10.30598//ijcr.2021.7-wul

[19] I. U. Haq, S. Amin, Lipoic acid-A short review, *Science International (Lahore)*, 19, 4, (2007), 273-276

[20] Daniel Martín-Yerga, Isabel Álvarez-Martos, M. Carmen Blanco-López, Charles S. Henry, M. Teresa Fernández-Abedul, Point-of-need simultaneous electrochemical detection of lead and cadmium using low-cost stencil-printed transparency electrodes, *Analytica Chimica Acta*, 981, (2017), 24-33 https://doi.org/10.1016/j.aca.2017.05.027

[21] Andres W. Martinez, Scott T. Phillips, George M. Whitesides, Emanuel Carrilho, Diagnostics for the Developing World: Microfluidic Paper-Based Analytical Devices, *Analytical Chemistry*, 82, 1, (2010), 3-10 https://doi.org/10.1021/ac9013989

[22] Weian Zhao, M. Monsur Ali, Sergio D. Aguirre, Michael A. Brook, Yingfu Li, Paper-Based Bioassays Using Gold Nanoparticle Colorimetric Probes, *Analytical Chemistry*, 80, 22, (2008), 8431-8437 https://doi.org/10.1021/ac801008q

[23] Deepak Varshney, Majid Ahmadi, Maxime J. F. Guinel, Brad R. Weiner, Gerardo Morell, Single-step route to diamond-nanotube composite, *Nanoscale Research Letters*, 7, (2012), 535 https://doi.org/10.1186/1556-276X-7-535

[24] Douglas A. Skoog, F. James Holler, Stanley R. Crouch, *Principles of instrumental analysis*, Seventh edition ed., Cengage Learning Australia, Australia, 2018,

[25] S. B. Eskander, H. M. Saleh, Wet oxidative degradation of cellulosic wastes: decomposition of waste protective clothes simulate, *Academic Journal of Chemistry*, 1, 3, (2016), 93-101

[26] Abraham Marmur, Volpe Claudio Della, Stefano Siboni, Alidad Amirfazli, Jaroslaw W. Drelich, Contact angles and wettability: towards common

and accurate terminology, *Surface Innovations*, 5, 1, (2017), 3-8 https://doi.org/10.1680/jsuin.17.00002

[27] Xuan Xie, Rudolf Holze, Electrode Kinetic Data: Geometric vs. Real Surface Area, *Batteries*, 8, 10, (2022), 146 https://doi.org/10.3390/batteries8100146

[28] Dennis H. Evans, Kathleen M. O'Connell, Ralph A. Petersen, Michael J. Kelly, Cyclic voltammetry, *Journal of Chemical Education*, 60, 4, (1983), 290 https://doi.org/10.1021/ed060p290

[29] R. C. Murray, P. A. Rock, The determination of the ferrocyanide—ferricyanide standard electrode potential at 25°C in cells without liquid junction using cation-sensitive glass electrodes, *Electrochimica Acta*, 13, 4, (1968), 969-975 https://doi.org/10.1016/0013-4686(68)85028-5

[30] O. A. González-Meza, E. R. Larios-Durán, A. Gutiérrez-Becerra, N. Casillas, J. I. Escalante, M. Bárcena-Soto, Development of a Randles-Ševčík-like equation to predict the peak current of cyclic voltammetry for solid metal hexacyanoferrates, *Journal of Solid State Electrochemistry*, 23, 11, (2019), 3123-3133 https://doi.org/10.1007/s10008-019-04410-6

[31] Zhiwei Lu, Junjun Zhang, Wanlin Dai, Xueni Lin, Jiaping Ye, Jianshan Ye, A screen-printed carbon electrode modified with a bismuth film and gold nanoparticles for simultaneous stripping voltammetric determination of Zn(II), Pb(II) and Cu(II), *Microchimica Acta*, 184, 12, (2017), 4731-4740 https://doi.org/10.1007/s00604-017-2521-8

[32] Alejandro García-Miranda Ferrari, Christopher W. Foster, Peter J. Kelly, Dale A. C. Brownson, Craig E. Banks, Determination of the Electrochemical Area of Screen-Printed Electrochemical Sensing Platforms, *Biosensors*, 8, 2, (2018), 53 https://doi.org/10.3390/bios8020053

[33] Sergio I. Martinez-Monteagudo, Electrochemical Analysis, in: P.L.H. McSweeney, J.P. McNamara (Eds.) *Encyclopedia of Dairy Sciences (Third Edition)*, Academic Press, Oxford, 2022, https://doi.org/10.1016/B978-0-12-818766-1.00340-8

[34] Neda Shahbazi, Rouholah Zare-Dorabei, A Facile Colorimetric and Spectrophotometric Method for Sensitive Determination of Metformin in Human Serum Based on Citrate-Capped Gold Nanoparticles: Central Composite Design Optimization, *ACS Omega*, 4, 17, (2019), 17519-17526 https://doi.org/10.1021/acsomega.9b02389

[35] AOAC International, Appendix F Guidelines for Standard Method Performance Requirements, in: G.W. Latimer, Jr. (Ed.) *Official Methods of Analysis of AOAC INTERNATIONAL*, Oxford University Press, 2023, https://doi.org/10.1093/9780197610145.005.006

[36] A. Fajgelj, Á. Ambrus, William Horwitz, The potential use of quality control data to validate pesticide residue method performance, in: A. Fajgelj, A. Ambrus (Eds.) *Principles and Practices of Method Validation*, The Royal Society of Chemistry, 2000, https://doi.org/10.1039/9781847551757-00001

[37] Gaviña Pablo, Parra Margarita, Gil Salvador, M. Costero Ana, Red or Blue? Gold Nanoparticles in Colorimetric Sensing, in: R. Mohammed, A. Abdullah Mohammed (Eds.) *Gold Nanoparticles*, IntechOpen, Rijeka, 2018, https://doi.org/10.5772/intechopen.80052